Waste Management 207 (2025) 115109

Contents lists available at ScienceDirect

Waste Management

journal homepage: www.elsevier.com/locate/wasman

Research Paper

A techno-economic evaluation of the hydrometallurgical recycling of mixed CAM black mass from spent LIB cells

Moritz Petzold [a,*], Dominik Büscher [b], Dzeneta Vrucak [b], Richard Woeste [c], Peter Hense [d], Sabine Flamme [a], Bernd Friedrich [b], Peter Letmathe [c]

[a] Institute for Infrastructure, Water Management, Resources and Environment, University of Applied Sciences Münster, Corrensstraße 25, 48149 Münster, Germany
[b] Institute for Process Metallurgy and Metal Recycling, RWTH Aachen University, Intzestraße 3, 52056 Aachen, Germany
[c] Chair of Management Accounting, RWTH Aachen University, Templergraben 64, 52062 Aachen, Germany
[d] Institute for Water, Environment and Energy, Bochum University of Applied Sciences, Am Hochschulcampus 1, 44801 Bochum, Germany

ARTICLE INFO

Keywords:
lithium-ion battery (LIB) recycling
Circular economy
Hydrometallurgical recycling
sensor-based sorting (SBS)
Battery cell chemistries
Total cost of ownership (TCO) analysis

ABSTRACT

The increasing diversity of lithium-ion batteries (LIBs) has introduced a range of cathode active materials (CAMs), with at least five major types currently in use. Regarding current recycling practices, end-of-life LIB cells are typically processed without any presorting, which results in a mixed CAM black mass input for hydrometallurgical treatment. This study evaluates the performance of a standard hydrometallurgical process under mixed CAM conditions and compares it with two hypothetical presorting scenarios by using a total cost of ownership (TCO) approach. Technically, the presence of lithium iron phosphate (LFP) black mass causes impurities that negatively affect process efficiency. Economically, the usage of partial presorting alone to recover cobalt-rich fractions results in a lower overall value compared to the mixed CAM baseline, due to the reduced marketability of the remaining material. However, further removal of LFP and lithium manganese oxide (LMO) improves both process quality and economic profitability, as most of the black mass can then be treated without major contaminants. The results also indicate that the hydrometallurgical process evaluated is not suitable for LFP recycling, thus highlighting the need for specific treatment strategies for phosphate-based chemistries.

1. Introduction

Lithium-ion batteries (LIBs) are a cornerstone technology for the decarbonization of modern society, in particular through the electrification of transport and mobility. With the expected growth in demand for LIBs, Europe is facing two key challenges: The supply of critical raw materials for LIB production, such as lithium, cobalt, and nickel, and the efficient management of increasing return volumes of spent LIBs (Schmaltz 2023). Several studies, such as Bobba et al. (2020), point out supply risks for key battery materials, such as cobalt, lithium, and graphite. New regulations, such as the EU Battery Regulation (EU 2023) and the EU Critical Raw Materials Act (EU 2024), are promoting the recycling of spent LIBs in the EU. These regulations set high recycling targets for critical metals to encourage investment in recycling infrastructure. To date, no standard recycling process has been established, although several approaches have been tested in laboratory and pilot-scale recycling facilities (Petzold and Flamme 2024). The general goal is to recover as much as possible of the valuable materials from the cathode active materials (CAMs). To this end, spent LIBs are typically crushed in rotary shear shredders, followed by sorting into different material fractions (Diekmann et al. 2017). The recovered black mass (BM), which accounts for approximately 50 % of the mass of an LIB cell (Arnberger et al. 2018), is then processed either pyrometallurgically or hydrometallurgically with an optional thermal pretreatment step to remove organic residues such as binders (Pinegar and Smith 2019). Due to high energy consumption, stand-alone pyrometallurgical recycling

Abbreviations: BM, Black mass; CAM, Cathode active material; Capex, Capital expenditures; EG8/9, Pay groups 8/9 according to collective agreement (Germany); ICP-OES, Inductively coupled plasma optical emission spectrometry; LCO, Lithium cobalt oxide; LFP, Lithium iron phosphate; LIB, Lithium-ion battery; LIBZ, Presorting scenario; LMO, Lithium manganese oxide; MVF, Mixed value factor; NCA, Lithium nickel cobalt aluminum oxide; NiCd, Nickel cadmium; NiMH, Nickel metal hydride; NMC, Lithium nickel manganese cobalt oxide; NPV, Net present value; OLS, Ordinary least squares; Opex, Operating expenditures; PGNAA, Prompt gamma neutron activation analysis; SBS, Sensor-based sorting; TCO, Total cost of ownership; WACC, Weighted average cost of capital; XRT, X-ray transmission.

* Corresponding author.
E-mail address: m.petzold@fh-muenster.de (M. Petzold).

https://doi.org/10.1016/j.wasman.2025.115109
Received 27 June 2025; Received in revised form 15 August 2025; Accepted 2 September 2025
Available online 12 September 2025

processes are no longer widely used, with the scale-up of recycling plants tending towards the hydrometallurgical route, which may include thermal pretreatment of the BM (Chen et al. 2022). Although a lot of research has been done on BM recycling, most of it has involved a single CAM type. In the processes, the BM (CAM types; LCO, NMC, LMO, NCA) is first leached with sulfuric acid and a reducing agent. The resulting leaching solution is then purified of copper, iron, and aluminum using various precipitation processes. Finally, the valuable metals cobalt, nickel, and also manganese are recovered from the leaching solution either by selective precipitation, co-precipitation, or solvent extraction, and in a final step, lithium is recovered by precipitation (Jung et al. 2021). There are various recycling approaches for the recovery of LFP-BM. (Müller and Obuz, 2024) have developed a hydrometallurgical process in which the BM is first thermally pretreated and then leached with phosphoric acid. Subsequently, the leaching solution is temperature adjusted to precipitate the dissolved iron and phosphate as iron phosphate ($FePO_4$), and the acid is returned to the leaching step. As a final step, lithium is precipitated as lithium phosphate (Li_3PO_4) (Müller and Obuz, 2024). Another option is to leach the thermally pretreated black mass using sulfuric acid, followed by precipitation of $FePO_4$ by adjusting the pH and lithium recovery using sodium carbonate (Na_2CO_3) as lithium carbonate (Li_2CO_3) ((Zheng et al. 2016). In addition, there are approaches such as selective leaching, salt leaching, electrochemical processes, and direct regeneration of LFP, e.g., using a molten salt process (Wen et al. 2024).The updated EU battery regulation aims to increase transparency, especially for the material composition of LIB. Through the battery passport, all batteries from electric vehicle, light means of transport and industrial batteries with a capacity of more than 2 kWh must provide information on material composition from the 1st of January 2026 onwards (EU 2023). However, this does not include all batteries produced before 2026 or even all portable batteries, which currently account for roughly half of the returning batteries (Schmaltz 2023). The missing information on CAM composition of spent LIB will result in a heterogeneous battery mix and needs to be addressed through presorting. This can be implemented by using different strategies. A distinction is made between manual, mechanical, and automated sorting (Sziegoleit 2013). In manual (or optical) sorting, spent batteries are sorted by humans on the basis of optical characteristics such as type designation or manufacturer. This is the current state in most European battery sorting facilities (Petzold and Flamme 2024). Mechanical sorting is carried out e.g., by sieve classification, where used batteries are sorted according to their size (Sziegoleit 2013). Automated sorting of batteries can be realized by using sensor-based sorting (SBS) systems. These can utilize several technologies, including optical, X-ray transmission, and X-ray fluorescence (Petzold and Flamme 2024).

Currently, such technologies are being used to sort spent batteries by electrochemical systems, such as LIB, NiMH, NiCd, etc. (Sterkens et al. 2021; Petzold and Flamme, 2025). In some research concepts, for example, LIB cells have been sorted into cobalt-rich and cobalt-poor fractions by using prompt gamma neutron activation analysis (PGNAA) (Sletsgaard and Pedersen 2014). Other literature demonstrates optical sorting based on character recognition to automate the sorting process and further sorting according to the CAM of spent LIB, and proposes X-ray sorting to exploit the different atomic densities of different CAMs (Bettersize Instruments Ltd. 2021). Research has also been published on the use of discharge data from spent LIBs to differentiate between lithium iron phosphate (LFP) and lithium nickel manganese cobalt oxide (NMC) cells (Wett et al. 2025). For spent LIB pouch cells, XRF characterization and sorting between LCO and NMC cathode also looks promising (Petzold et al. 2024). In the present paper, a total cost of ownership (TCO) approach is used to evaluate the need for CAM sorting through different sorting strategies.

The research questions to be answered are:

(1) What factors influence the technical and economic advantageousness of the hydrometallurgical recycling of LIB cells at the end of their lifecycle?
(2) How can a presorting step improve the hydrometallurgical recycling of spent LIB cells?

This paper is structured as follows. Section 2 provides a brief overview of the different CAMs used in LIBs and potential hydrometallurgical recycling processes for spent LIBs. Market prices for materials and process auxiliaries, possible presorting scenarios, and the TCO model for further calculations are described in Section 3. TCO results for the different presorting scenarios as well as sensitivity analyses assessing the potential influence of each CAM in the processed BM mix are presented in Section 4. The paper concludes with a discussion of the results and limitations of this work as well as an outlook on future developments in hydrometallurgical recycling processes.

2. Material and methods

In this section, different presorting strategies and the hydrometallurgical recycling process to be evaluated are described from a technical point of view. In addition, the TCO method is briefly explained.

2.1. Lithium-ion batteries and cathode active materials

LIB cells typically consist of two electrodes (anode and cathode), an electrolyte, and a separator membrane. All commercially available LIBs use aluminum (cathode) and copper (anode) as current conductors. The most commonly used anode active material in commercial applications is graphite, although lithium metal can also be used (Zhang et al. 2021; Wurm et al. 2013; Wu 2002). During the last 30 years of LIB development, several CAMs have been developed and are being used in commercially available LIB cells. Most of them use either transition metal oxides or polyanion compounds, due to their high operating voltages and the resulting high storage capacity (Nitta et al. 2015). The five dominant CAMs used in commercial applications are lithium cobalt oxide ($LiCoO_2$, LCO), lithium manganese oxide ($LiMn_2O_4$, LMO), lithium nickel manganese cobalt oxide ($LiNi_xMn_yCo_zO_2$, NMC), lithium nickel cobalt aluminum oxide ($LiNi_XCo_YAl_ZO_2$, NCA), and lithium iron phosphate ($LiFePO_4$, LFP). While LCO is mostly used in consumer applications for cell phones, tablets, and laptops, LFP, NCA and NMC are primarily used in electric vehicles. LFP is also applied in battery storage systems. NCA is the most common CAM used in US electric vehicles, such as Tesla (Zhao et al. 2022); NMC is mainly used in European cars, while LFP is predominantly used in China and other Asian countries (Zhao et al. 2022).

2.2. Hydrometallurgical recycling

An exemplary hydrometallurgical recovery process for BM recycling (see Fig. 1) was used as a reference for analyzing the effects of these presorting scenarios in order to determine whether the presorting of LIB cells into fractions of different CAMs is necessary and how it affects further processing.

To evaluate the effects on the hydrometallurgical recycling process, the individual battery types were first pretreated mechanically and then thermally. The first step was wet shredding in an adapted cutting mill (type SM 300, Retsch GmbH, Haan, Germany), which was equipped with a 6-disc rotor (stainless steel with reversible tungsten carbide cutting tips) and a bottom sieve with 8 mm square holes. Using a small pump (Syncra Silent 3.0, Sicce S.r.l., Pozzoleone, Italy) the entire shredding mill was continuously purged with process water to ensure safe conditions for the opening and the comminution of the LIB cells. After completion, core particles > 0.5 mm were separated using a laboratory sieve. The resulting BMs were then dried in a drying oven at 105 °C for 24 h to ensure easier handling through pyrolysis. Pyrolysis is a crucial

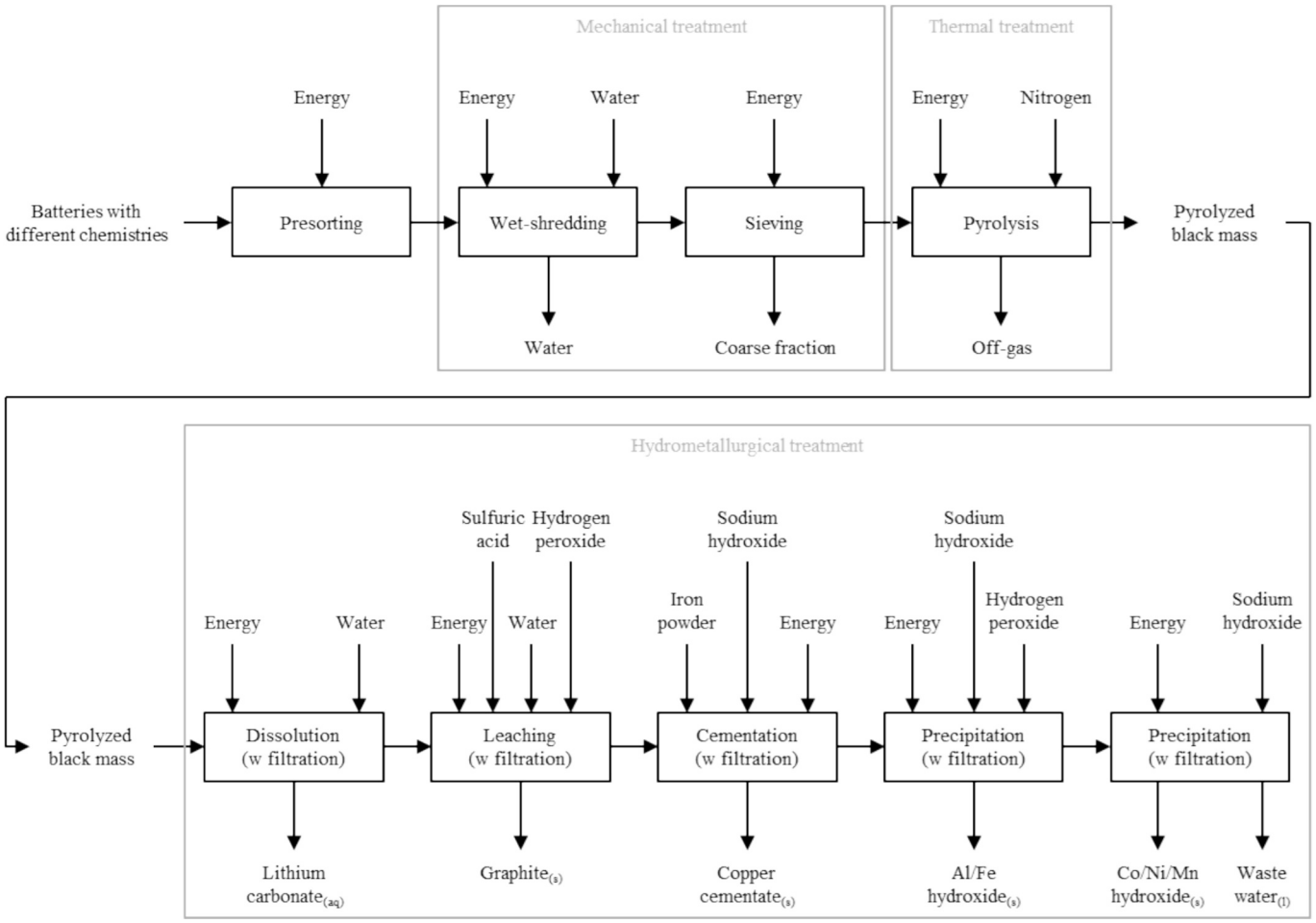

Fig. 1. Investigated hydrometallurgical process route (own figure).

step in the pretreatment of BM, not only to volatilize organic matter (e.g., binder, separator, electrolyte) but also to transform lithium oxide into water-soluble lithium carbonate (Qiu et al. 2024; Tao et al. 2021). For this purpose, the BMs were placed in a crucible inside a resistance-heated furnace (Thermo-Star Experimental Furnace, Thermo-Star GmbH, Aachen, Germany) and heated under continuous nitrogen flow (5 l/min) at a heating rate of 300 °C/h to a target temperature of 600 °C. Upon reaching the target temperature, a holding time of 60 min was maintained. The process parameters were selected based on several studies that had already been performed and that had identified these parameters as optimal (Stallmeister and Friedrich 2023; Babanejad et al. 2022; Yang et al. 2016). This can be explained by the required temperature of at least 500 °C for the decomposition of the binder and at least 600 °C for the reduction of the lithium metal oxides (Babanejad et al. 2022). After the holding time, the furnace was turned off, and the BMs remained inside the furnace until room temperature was reached. The pyrolyzed black masses were then combined into different mixed fractions according to the presorting scenarios derived in Section 3.2, and they were further processed in the hydrometallurgical treatment.

In the first step of the hydrometallurgical treatment, the conversion of lithium into water-soluble lithium carbonate during pyrolysis plays a crucial role. Although lithium carbonate has a limited solubility in water (13.4 g/L), this property can be utilized to selectively dissolve lithium and separate it from other metals (Qiu et al. 2024). For better differentiation of the process steps and because there is no physical change in the lithium carbonate, the process step investigated here is called “dissolution”. The dissolution parameters were as follows: 1:30 solid to liquid ratio (s/l), 25 °C, 300 rpm. In the following leaching step, a mixture of sulfuric acid (2 M) and hydrogen peroxide (4 vol%) was used to dissolve nickel, cobalt, and manganese. The lithium-free black mass was leached at 60 °C for 2 h at 250 rpm with an s/l of 1:10. Several studies have been conducted using similar parameters and showing high leaching efficiencies (> 95 %) of cobalt, nickel, and manganese (Saleem et al. 2023; Zheng et al. 2017; Zhu et al. 2012; Sun and Qiu 2011). Residual copper in the BM was also dissolved by adding hydrogen peroxide. To selectively recover copper, cementation can be conducted. During this step, sodium hydroxide was added to raise the pH to above 1 (here: to exactly 1.15) at 60 °C. Iron is usually added in proportion to the amount of copper in solution. Due to the heterogeneity of the input BM mixtures, the same amount of iron was added to each solution, so 10 g/L of the initial leaching solution volume was added to each solution. The added iron was removed in the subsequent precipitation step, which serves as purification of the loaded solution. The process parameters of the purification precipitation to remove aluminum and iron as hydroxides were as follows: a pH of 3.8, a temperature of 60 °C, and the addition of hydrogen peroxide at 1 vol%. The final precipitation to recover nickel, manganese, and cobalt as hydroxides was carried out at room temperature and at pH 11. For the sample, 50 mg of black mass was dissolved in reversed *aqua regia* using a Multiwave 7000 (Anton Paar, Graz, Austria) microwave digestion system prior to analysis. The stoichiometry and the chemical composition of the samples were determined by ICP-OES using an ARCOS (Spectro Analytical Instruments GmbH, Kleve, Germany) equipped with a Scott spray chamber, a cross-flow nebulizer, and an axially positioned plasma torch (Gnutzmann et al. 2024). The method and further parameters were adapted from Evertz et al. (2019) and Vortmann-Westhoven et al. (2017).

2.3. Net present value and total cost of ownership

The TCO method allows the evaluation of all costs incurred during the life cycle of a product or, as in the paper at hand, the execution of a process (Ellram and Siferd 1993). A TCO model takes into account all cash-effective capital expenditures (Capex) as well as all operating expenditures (Opex) associated with the process (Ferrin and Plank 2002; Degraeve et al. 2000; Degraeve and Roodhooft 1999; Ellram 1995, 1994). The method therefore takes a holistic approach to the asset under consideration (Degraeve et al. 2000; Ellram 1995). Since the cost structure is specific to the individual asset under consideration, the TCO model is not universal for every product or process, but must always be adapted to the specific application (Bhutta and Huq 2002; Ferrin and Plank 2002). Accordingly, the calculation presented in the current paper also considers, for example, the revenues generated from recycled product sales. The main challenge of the TCO method is the need for detailed data and the uncertainty in estimating cost drivers to obtain reliable results (Geissdörfer et al. 2009; Degraeve et al. 2000; Ellram 1995). Accordingly, the results should be subjected to sensitivity analysis.

The annual TCO is the annuity of the net present value (NPV) as shown in Eq. (1), where T is the total time horizon and i is the discount rate:

$$TCO = NPV\frac{(1+i)^T i}{(1+i)^T - 1} \tag{1}$$

The NPV includes the initial capital expenditure C_{Capex} in $t = 0$ as well as annual operating expenditures $C_{\mathrm{Opex},t}$ and revenues R_t. In Eq. (2), again T is the total time horizon and i is the discount rate:

$$NPV = -C_{Capex} + \sum_{t=1}^{T}\frac{R_t - C_{Opex,t}}{(1+i)^t} \tag{2}$$

It is assumed that no assets require replacement during the period under review and that they possess no residual value at the conclusion of this period. Consequently, Capex are exclusively incurred as initial costs and not on a recurring basis.

3. Theory and calculation

After discussing the material and auxiliary material prices in Section 3.1 and defining the price development scenarios, the presorting scenarios for further calculations are derived in Section 3.2. Finally, in Section 3.3, the TCO model is set up to evaluate the previously defined process scenarios.

3.1. Material and auxiliary prices

LIB recycling processes have inherently high Opex, as the main process stream is a mixture of high-value materials. In addition, especially for hydrometallurgical processes, a variety of process auxiliaries are required as described in Section 2.2. Therefore, accurate estimates of the respective material prices are necessary to obtain well-fitting overall results for the economic analysis of the process. Considering the long period of 25 years, four different price scenarios are defined to reflect different future developments and to facilitate decision making under this uncertainty. All of them start from the same value p_j within the first year and, depending on the price development scenario, different price growth rates g_j are applied. Specifically, the four scenarios are: a fixed scenario with no price changes over time ($g_j = 0$), and a lower, a base, and an upper scenario, each scenario with increasing values of g_j for each material j, respectively.

Consistent with our previous works on the evaluation of LIB recycling processes (Woeste et al. 2024; Reinhart et al. 2023), a log-linear ordinary least squares (OLS) regression was used to obtain the price growth rates for the lower price development scenario based on historical price data sets. In cases where no data on price history data were available, the price growth rate in the lower scenario was set to zero. For the base and the upper price development scenarios, 0.01635 and 0.02811 were added, respectively, to the values in the lower scenario. These values were chosen because they reflect overall price increases of 150 % and 200 %, respectively, over the 25-year period considered. Potential causalities or correlations between the development of individual materials may be inherent in the data but are not explicitly considered in the calculations. The price growth rates have been constrained to zero as a lower bound and safe estimate, and to 0.07189, 0.08824, and 0.1 as upper bounds in the lower, base, and upper scenarios, respectively. The differences between the upper bounds of the scenarios reflect the differences of 0.01635 and 0.02811 mentioned above. For the materials considered in this paper, the limits were only relevant for Li_2CO_3, $Co(OH)_2$, H_2O_2, and solid waste in the lower scenario (0.10042, –0.00752, –0.00072, and –0.00130) and for Li_2CO_3 in the base and upper price development scenarios (0.11677 and 0.12853).

In general, price data are derived from the German balance of foreign trade from 01/2006 to 11/2024, for which prices are reported monthly (Destatis 2025a). The respective starting price for the initial year is the average price for each material in 2024, which is the last year available in the price data set. Eurostat data from 2007 to 2024 resulted in estimates for electricity prices (Eurostat 2025). The range between 2 GWh and 20 GWh per year was used, as it best reflects the power consumption of the considered processes. Water costs are taken from utility data assuming a consumption of between 30,001 m^3 and 100,000 m^3 per year based on process data (Stawag 2025). Prices for electrolyte disposal, carried out by waste incineration, Al/Fe hydroxide disposal, which includes immobilization of Al/Fe hydroxide sludge and the subsequent disposal via a specialized waste management company (other possibilities for recycling Al/Fe hydroxide include thermal treatment and further use, e.g., in road construction (Hoeber and Steinlechner, 2021)), and wastewater treatment, including heavy metal precipitation and Glauber's salt crystallization followed by discharge into a local wastewater treatment plant, are based on own experience. Appendix B provides an overview of the initial prices for each material and of the respective price growth rates for the scenarios other than the fixed price scenario.

For mixed output fractions, the prices are calculated using a weighted average price according to the proportion of the mixture. As all price data refer to pure substances, a mixed value factor MVF_j was applied to the sales prices of each process output j depending on the mass fraction w_j of the desired product within the output, as shown in Eq. (3). This approach resulted from discussions with experts in the field.

$$MVF_j(w_j) = 0.25 \bullet 4^{w_j}, \forall w_j \in [0,1] \tag{3}$$

3.2. Presorting scenarios

To discuss the effect of presorting LIB cells according to their CAM, different presorting scenarios (LIBZ) were evaluated. Various methods have been tested for sorting battery cells (TOMRA 2021; Sziegoleit 2013), with X-ray transmission (XRT) being one of the most promising approaches (Petzold and Flamme 2024). For the paper at hand, different presorting scenarios were derived based on a conceptual analysis of XRT presorting. Each scenario represents a theoretically plausible approach that could be implemented depending on the available sensor systems, the level of automation, and the intended downstream application. The evaluation of the scenarios was aimed at exploring the impact of different presorting depths on the hydrometallurgical processing routes for mixed BM. The economic value of CAMs is mainly based on the amount of cobalt and nickel they contain, the value of which is 8 to 12 times higher than that of aluminum and manganese (LME 2025a, 2025b). Therefore, the removal of LCO in the first step is reasonable (LIBZ2.1), while LFP, LMO, NCA, and NMC make up the residual

(LIBZ2.2).

LFP and NMC should be separated, as a hydrometallurgical processing of the two of them together results in high losses (Krüger et al. 2014). Therefore, the second step is the removal of LFP and LMO (LIBZ3.1) from the high quality NMC/NCA fraction (LIBZ3.2). Preliminary tests have shown that the separation of these CAMs is quite difficult, with some NCA remaining in the LFP/LMO residue. Further presorting into individual CAMs is not considered, as the atomic densities of both LFP/LMO and NMC/NCA are quite similar, and presorting would be hardly possible. There have been various market analyses looking at the market shares of the most common CAMs, e.g., Melin (2018). For the present paper, the market shares from Melin (2018) for 2025 are used (see LIBZ1 in Table 1), which form the basis for the composition of the three examined presorting scenarios shown in Fig. 2.

3.3. TCO model

The economic evaluation of the proposed LIB presorting and recycling processes is based on a comprehensive TCO model, which has the same structure for the different presorting scenarios. This structure is shown in Fig. 3 and includes capital expenditures, operating costs, as well as revenues from the sale of output fractions.

The initial investment consists of buildings and various technical equipment, including shipping and installation costs. The relevant data regarding technical equipment are taken from previous studies and offers, and have been updated where necessary and adjusted for inflation to 2024 using data from Destatis (2025b). Based on own experience, a useful life of 25 years without the need for replacement of the technical equipment is a valid assumption. The calculation of capital expenditures for the buildings is based on BKI (2024) cost estimates for institute and laboratory buildings. As hydrometallurgy has been identified as the bottleneck in the overall process route, all other upstream process steps have been designed based on the capacity of 500 kg/h of the hydrometallurgical process step equipment to achieve full utilization there. This results in a capacity of the entire considered process route of 1,000 kg LIB cells per hour. Only buildings and technical equipment directly related to the process route considered are included in the TCO calculation. However, general equipment for the directly required buildings, such as cranes, workplace equipment and furniture, safety equipment including off-gas and wastewater treatment, if required in the individual process steps, are not excluded from the further calculations. This amounts to an initial investment of approximately 34.3 million € (33.6 million € without presorting). The technical equipment accounts for 53.28 % of this (52.91 % without presorting). The main components of the technical equipment for each process step and an overview of the distribution of the initial investments in each process step are presented in Appendix C.

Operating costs include both variable and fixed costs. The latter include labor, maintenance, and insurance costs. The calculation of wage costs is based on an average wage from wage groups EG8/9 (IG Metall 2024a). In Germany, social security contributions are due in addition to wages and must be included in the employer's wage cost. The social security contributions include 18.6 % for pension insurance,[1] 14.6 %[2] plus an additional 2.5 % for health insurance (BMG - Bundesministerium für Gesundheit, 2024), 3.6 % for long-term care insurance,[3] and 2.6 % for unemployment insurance.[4] Depending on the respective activities,[5] the employer must also contribute to accident insurance, which is assumed to be 1 % at this point. Social security contributions are largely borne equally by the employer and the employee. In detail, this results in a surcharge of 21.95 % on the gross wage for the employer's social security contributions. Other surcharges to be considered are 15 % for late shifts and 25 % for night shifts (IG Metall 2024b), as three-shift operation is planned, and 70 % of a gross monthly salary as vacation pay (IG Metall 2011). Overall, the employer's wage costs for an average position in the process considered here add up to 57,221.70 € per year. Wages are kept constant over time in all scenarios.[6] A total of 20 employees are required. See Appendix C for details of each process step. Maintenance and insurance costs for buildings and technical equipment are annual payments and are calculated as a percentage of the respective initial investment. The markups (buildings: 1.5 % for maintenance and 1 % for insurance; technical equipment: 3 % for maintenance and 1 % for insurance) are taken from Bärwaldt and Kwade (2012) and adjusted based on expert knowledge.

Variable costs include material costs, energy costs, and the cost of disposal of waste streams and wastewater treatment. The price data on which the calculations are based are described in Section 3.1. These are multiplied by the corresponding material and energy flows to obtain the absolute values per year. Since no costs are considered for the purchase of end-of-life LIB cells, the TCO per ton of LIB cells shown later in the results can be understood as the break-even price per ton of LIB cells to be recycled. If the price is higher than the respective value, the process would not be considered financially profitable. Appendix C provides an overview of the variable costs and revenues associated with each step. The variable costs as well as the revenues from output fractions depend directly on the production times per year. In the scale assumed here, 250 working days per year and thus 6,000 h per year are assumed. The actual production time is 5,700 h per year, since 5 % of the time is scheduled for maintenance and set-up time.

The annual cash flows resulting from the costs and revenues are discounted at a rate of 8.4 %. This rate is derived from the weighted average cost of capital (WACC) for the materials industry in February 2025 (PwC 2025).

Table 1
Market shares according to CAM for 2025, based on Melin (2018), and presorting scenarios (own table).

	LIBZ1	LIBZ2.1	LIBZ2.2	LIBZ3.1	LIBZ3.2
LCO	35.7 %	100.0 %	./.	./.	./.
LFP	35.7 %	./.	55.6 %	83.2 %	./.
NMC	13.3 %	./.	20.8 %	./.	62.5 %
NCA	9.6 %	./.	14.9 %	3.7 %	37.5 %
LMO	5.6 %	./.	8.7 %	13.0 %	./.

4. Results and discussion

In the following section the results of the TCO calculation are presented and discussed. The focus is on the impact of the different presorting and price development scenarios. The results are further evaluated in sensitivity analyses, where the influence of variations in the MFV is analyzed.

4.1. TCO results

Assuming an observation period of 25 years and a throughput of 5,700 t of LIB cells per year, a mixed picture emerges regarding the

[1] See § 1 BSV 2018 in Bundesregierung Deutschland 2018.
[2] See § 214 SGB V in Deutscher Bundestag 1989.
[3] See § 55(1) SGB XI in Deutscher Bundestag 1995.
[4] See § 341(2) SGB III in Deutscher Bundestag 1998.
[5] See § 153(1) SGB VII in Deutscher Bundestag 1997.
[6] The impact of wage increases on price development scenarios was examined. Wage increases in line with the aforementioned default price increases lead to less profitable processes in the base and high scenarios, and no changes in the fixed and low scenarios. Only LIBZ1 and LIBZ2 show a change in sign for the base scenario.

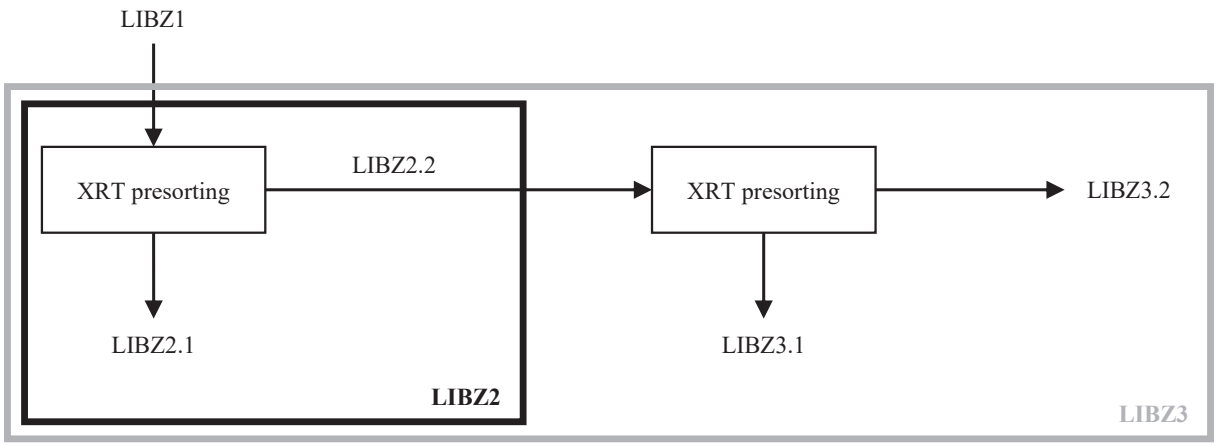

Fig. 2. Presorting scenarios and respective sorting fractions considered (own figure).

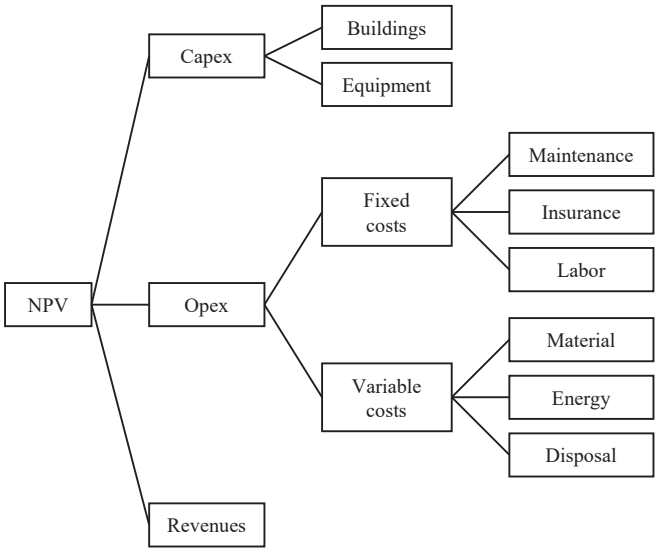

Fig. 3. TCO model (own figure).

economic feasibility of recycling LIB cells. The results for all presorting scenarios and all price development scenarios are shown in Table 2. As described in Section 3.3, the results represent break-even values for the purchase of the end-of-life LIB cells to be recycled, as the costs incurred for this are not included in the TCO model. If the cost of the LIB cells to be processed is less than the specified TCO per ton of LIB cells, the process is profitable in the respective scenario. However, this also means that if the values are negative, a fee would have to be paid to the recycler to make recycling profitable. Looking at the results, it is noticeable that the economic feasibility of the recycling process improves both from the fixed price development scenario to the upper price development scenario and from the LIBZ1 to the LIBZ3 presorting scenario, with LIBZ2 being slightly worse than LIBZ1.

The first trend can be explained by the fact that product revenues increase more than raw material costs over all four price development scenarios. Although the price of process materials, such as NaOH or H_2SO_4, and the price of electricity rise sharply, this can be over-compensated by the price trends for the output fractions, especially when the different starting prices are considered.

The second trend is due to the tendency for the mass yield weighted by MVF, which depends on the product purity, to increase over the three presorting scenarios. The product purity of the Li_2CO_3 and graphite weighted according to the presorting sub-scenarios decreases slightly across the presorting scenarios. Although the output of cement Cu plays

Table 2
NPV and TCO results for all presorting and price development scenarios (own table).

Price scenario		Presorting scenario		
		LIBZ1	LIBZ2	LIBZ3
Fixed	NPV	–22,270,781.16 €	–22,646,226.82 €	–11,791,643.95 €
	TCO/a	–2,158,040.23 €	–2,194,420.94 €	–1,142,611.11 €
	TCO/t LIB cells	–378.60 €	–384.99 €	–200.46 €
Lower	NPV	–4,877,030.74 €	–7,168,375.30 €	3,408,839.02 €
	TCO/a	–472,584.61 €	–694,616.06 €	330,316.74 €
	TCO/t LIB cells	–82.91 €	–121.86 €	57.95 €
Base	NPV	4,319,483.90 €	1,138,383.99 €	13,032,383.26 €
	TCO/a	418,558.29 €	110,309.49 €	1,262,838.84 €
	TCO/t LIB cells	73.43 €	19.35 €	221.55 €
Upper	NPV	14,593,737.90 €	11,369,179.83 €	24,519,984.87 €
	TCO/a	1,414,134.21 €	1,101,674.31 €	2,375,988.22 €
	TCO/t LIB cells	248.09 €	193.28 €	416.84 €

a minor role from an economic point of view, it can nevertheless be seen that the product purity improves significantly across the presorting scenarios. For Ni/Co/Mn hydroxide, the concentration of the desired fraction in the output is slightly lower in the second scenario than in the first scenario but rises slightly above the value of the first scenario in the third scenario. However, the effect of increasing product purity on the result of the economic analysis is increased exponentially by the MVF function from Eq. (3) with increasing product purity, so this slight increase in the third scenario has an impact on the overall result. The development of the weighted product purities of the output fractions over the three presorting scenarios is shown in Table 3. Looking at the development of the mass yields achieved (see Table 3), there is a clear increase in cement Cu across the presorting scenarios as well as an increase in the $Co(OH)_2$ yield, the latter being much more relevant for the economic feasibility analysis. On the other hand, the yields of $Ni(OH)_2$ and $Mn(OH)_2$ both decrease. Regarding Li_2CO_3 and graphite, the picture is more mixed. The Li_2CO_3 yield is higher, and the graphite yield is lower in the second scenario compared to the first presorting scenario, while the opposite is true in the third scenario.

Overall, the improvement in the mass yield combined with the

Table 3
Development of the weighted product purities and mass yields over the presorting scenarios (own table).

Weighted product purities		
Output fraction	LIBZ1 → LIBZ2	LIBZ1 → LIBZ3
Li_2CO_3	–0.16 %	–1.44 %
Graphite	–2.67 %	–3.87 %
Cement Cu	+52.48 %	+195.76 %
Ni/Co/Mn hydroxide	–6.76 %	+0.21 %
Mass yields		
Output fraction	LIBZ1 → LIBZ2	LIBZ1 → LIBZ3
Li_2CO_3	+3.23 %	–1.38 %
Graphite	–3.16 %	+0.18 %
Cement Cu	+67.36 %	+243.75 %
$Ni(OH)_2$	–26.79 %	–9.26 %
$Co(OH)_2$	+1.89 %	+5.38 %
$Mn(OH)_2$	–29.92 %	–19.36 %

change in product purity, especially for the important fraction of $Co(OH)_2$, through presorting clearly exceeds the additional initial investment in equipment and buildings for presorting as well as the associated Opex when comparing LIBZ3 to LIBZ1. However, for LIBZ2, the effect of presorting the LIB cells cannot compensate for the additional expenditure for the presorting facility. LIBZ2 therefore lags behind LIBZ1 from an economic perspective in all price development scenarios.

The most important cost categories in the recycling process considered in this paper are energy and materials, which represent 31–40 % and 24–33 % of the total costs, respectively, depending on the scenario. Looking at the process steps, hydrometallurgy is by far the most expensive process step, accounting for 78–86 % of the total costs. In comparison, the share of the presorting process is less than 2.6 % in the scenarios where presorting takes place. Detailed cost shares can be found in Table 13 in Appendix C.

4.2. Sensitivity analysis

Material costs are the second largest cost category but are also a complex area due to the wide variety of input and output streams. Since the choice of MVF for each output fraction has a direct impact on the revenue earned from that output stream, sensitivity analysis of the impact of the MVF on the overall results is important. Since energy costs are the largest cost category, variations in energy prices are also part of the sensitivity analysis.

The MVF on each marketable output stream can take on values of between 0.25 and 1 according to Eq. (3). However, discounts of up to 100 % are possible. Therefore, in the following sensitivity analyses, a range between 0 and 1 is used for the MVF, where a MVF of 0 represents a product that does not generate any revenue but also does not lead to any disposal costs, and an MVF of 1 represents a product that can be sold at pure material market values. Both extreme cases are rather unlikely in real market conditions. Because the MVF is a factor applied to a revenue stream, varying its value leads to linear graphs when plotting TCO per ton of LIB cells processed. Fig. 4 shows the slopes of these relationships, representing the absolute change in results in EUR per percentage point change in the MVF of each output fraction, ceteris paribus.

The values indicate that the different presorting scenarios have a negligible effect on the sensitivity of the process to MVF changes. In the case of the MVF for Li_2CO_3 and graphite, this can be seen from the constant slopes across the presorting scenarios and is due to the comparatively small changes in product purity and mass yield between the presorting scenarios for these output fractions. In the case of cement Cu, although there is a clear increase in the slopes from LIBZ1 to LIBZ3, the level at which the values lie is very low, so that although there is an increasing sensitivity regarding MVF variations, this in fact has little effect on the result of the economic analysis. In the case of Ni/Co/Mn hydroxide, LIBZ1 and LIBZ3 are at a similar level, but for LIBZ2 the sensitivity of the result to MVF variation is lower than for the other two presorting scenarios.

The effect of an actual change in the MVF of each output fraction on the economic feasibility of the overall process is most easily determined

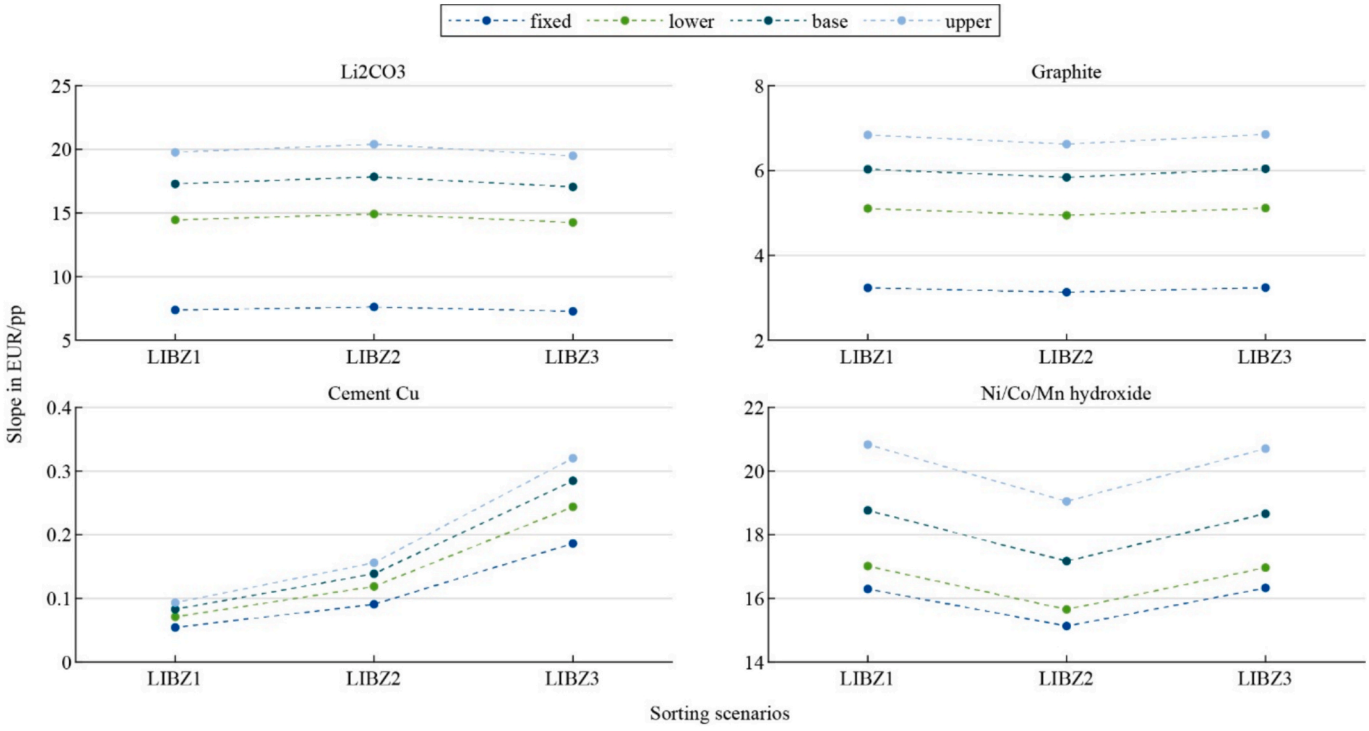

Fig. 4. Slopes of TCO per t of LIB cells processed with varying MVF for all presorting and price development scenarios, dashed lines to illustrate trends only (own figure).

by a break-even analysis. The corresponding results of these calculations are shown in Table 4. The values shown represent the MVF that would have to be present for the TCO per ton of LIB cells processed to be zero. Cases where the break-even MVF takes on unrealistic values of below 0 or above 1 are indicated by corresponding markers. Scenario combinations that have a positive TCO per ton of LIB cells processed in the results presented in Section 4.1 are marked in gray. In these cases, the aggregate MVFs used in the initial calculations are higher than the break-even values; in the other cases, the opposite is true. This also illustrates that a change in the MVF for cement Cu never leads to a change in the sign of the results presented in Section 4.1, that the fixed price scenario can never be positive, except in one case, and that the other cases with a negative result can only be turned positive by changes in the MVF for Ni/Co/Mn hydroxide or by an MVF for graphite close to 1. See Appendix D for detailed charts showing the impact of MVF changes on the TCO results.

To assess the impact of changes in the energy price on the results, electricity price changes ranging from –100 % to + 100 %, relative to the price used for the calculations, are considered. Since electricity consumption differs only in terms of the presence of presorting in scenarios LIBZ1 to LIBZ3, the slope of the TCO per ton of LIB cells processed with varying electricity prices for LIBZ2 and LIBZ3 is identical in each of the four price development scenarios (see Table 5). The slope for LIBZ1 is slightly flatter in each case because no presorting is carried out and the corresponding energy costs are not incurred. Table 5 also shows the break-even electricity price deviations necessary to make the TCO per ton of LIB cells processed zero. Fig. 9 in Appendix D shows a detailed chart illustrating the influence of electricity price changes on TCO results.

Table 4
MVF break-even values for all scenarios (own table).

Output fraction	Presorting scenario	Actual MVF from calculation	Price development scenario			
			Fixed	Lower	Base	Upper
Li_2CO_3	LIBZ1	0.963	○	○	0.920	0.837
	LIBZ2	0.961	○	○	0.957	0.873
	LIBZ3	0.945	○	0.941	0.852	0.768
Graphite	LIBZ1	0.833	○	0.995	0.711	0.470
	LIBZ2	0.809	○	○	0.774	0.515
	LIBZ3	0.798	○	0.682	0.429	0.187
Cement Cu	LIBZ1	0.278	○	○	●	●
	LIBZ2	0.293	○	○	●	●
	LIBZ3	0.344	○	●	●	●
Ni/Co/Mn hydroxide	LIBZ1	0.696	0.928	0.744	0.656	0.576
	LIBZ2	0.671	○	0.889	0.795	0.705
	LIBZ3	0.728	○	0.856	0.770	0.688

●: break-even below 0; ○: break-even above 1.

Table 5
Results of the sensitivity analysis regarding changes in energy price (own table).

Price development scenario	Slope in EUR/pp		Break-even electricity price deviation		
	LIBZ1	LIBZ2, LIBZ3	LIBZ1	LIBZ2	LIBZ3
Fixed	–10.33	–10.41	–36.64 %	–37.00 %	–19.26 %
Lower	–14.40	–14.50	–5.76 %	–8.40 %	+4.00 %
Base	–16.88	–17.00	+4.35 %	+1.14 %	+13.03 %
Upper	–19.04	–19.17	+13.03 %	+10.08 %	+21.74 %

5. Conclusion

This study evaluated three conceptual presorting scenarios for end-of-life LIBs within a standard hydrometallurgical recycling process and assessed their economic implications. Despite inherent limitations in process modeling and assumptions, clear trends emerged regarding the influence of presorting on the processing of mixed CAM black mass. Key factors affecting technical and economic viability include the hydrometallurgical recovery efficiencies of cobalt, lithium, nickel, and manganese. Among the scenarios, LIBZ2 was found to be the least favorable due to the low recovery out of the mixed CAM sub-fraction LIBZ2.2, outweighing gains from the high purity LCO fraction LIBZ2.1. In contrast, removing LFP and LMO in LIBZ3 significantly improved technical and economic outcomes, highlighting the need to separate LFP before hydrometallurgical treatment. The mass fraction of LFP to NMC mostly influences this during leaching, specifically a mass fraction of LFP above approximately 50°% has a negative effect (Pagnanelli et al. 2024). Additionally, a high s/l ratio of more than 70 g/l can also influence the leaching performance negatively (Hubert et al. 2025). Both apply to the leachings investigated and may be due to the re-oxidation of the valuable metals by a high concentration of ferric ions (Fe^{3+}), similar to the oxidation of copper by Fe^{3+} (Hughes 1970)). In addition, catalytic decomposition of H_2O_2 by Fe^{3+} may occur (Zou et al. 2024a). In the subsequent Cu-cementation, excessively high proportions of Fe^{3+} can lead to the re-oxidation of Cu^0(s) to Cu^{2+}(l), significantly reducing copper separation and resulting in copper impurities in subsequent processes, which substantially impair yield and purity (Garry Maurice Hughes 1970)). In addition to the problems already mentioned, the high iron concentration can lead to the formation of so-called iron hydrogels (J. Dousma und P.l. De Bruyn 1976) when removing iron using NaOH, which results in a high loss of the valuable metals, as a large amount of the leaching solution remains in the solid residue. The increased concentration of phosphate during leaching and subsequent purification of the solution also affects the precipitation of iron and aluminum, as it leads to co-precipitation of the valuable metals (Zou et al. 2024b). Establishing an optimized recycling process for LFP could increase the profitability of LIBZ2. The growing share of LFP-based batteries makes their separation from mixed streams increasingly important, particularly for cobalt recovery. LMO, though less harmful than LFP, adds little value and may warrant removal. Presorting improved both mass balance and product quality, with the largest yield gain in the copper cement fraction and notable value increases for Ni/Co/Mn hydroxides. The potential for improving purity and thus increasing value becomes clear when comparing Table 6 and Table 7 in the appendix. In this context, future research should also focus on the additional separation of NMC and NCA cells to further optimize material recovery and purity. In addition, the single-type LFP batteries can be subjected to specific recycling processes as described in the introduction. Since beyond the scope of this stuy, future work should address not only LFP and LMO separation but process engineering challenges, such as pumpability and filterability. Also, the processes could also be evaluated from an ecological perspective as part of a life cycle assessment in the future. Overall, the article demonstrates the need for presorted LIB by CAM to achieve a higher level of purity and yield. To this end, sensor-based sorting can be employed. However, changing the current battery regulations to make battery passports mandatory for all LIBs, including portable ones, could achieve similar or even better results.

CRediT authorship contribution statement

Moritz Petzold: Writing – original draft, Methodology, Formal analysis. **Dominik Büscher:** Writing – original draft, Methodology, Formal analysis. **Dzeneta Vrucak:** Writing – original draft, Methodology, Formal analysis. **Richard Woeste:** Writing – original draft, Methodology, Formal analysis. **Peter Hense:** Writing – original draft. **Sabine Flamme:** Writing – review & editing, Supervision. **Bernd Friedrich:** Writing – review & editing, Supervision. **Peter Letmathe:** Writing – review & editing, Supervision.

Declaration of competing interest

The authors declare the following financial interests/personal relationships which may be considered as potential competing interests: Moritz Petzold reports administrative support and article publishing charges were provided by FH Münster. If there are other authors, they declare that they have no known competing financial interests or personal relationships that could have appeared to influence the work reported in this paper.

Acknowledgments

The authors would like to thank Julius Buchmann (Münster Electrochemical Energy Technology (MEET), University of Münster, Germany) for conducting the ICP-OES analysis, which provided essential data for the evaluation of material recovery in this study.

Appendix A. .: Distribution factors

.

Table 6
Distribution factors of each process step and considered elements in % (own table).

LIBZ	Element	Dissolution in		Leaching in		Cementation in		Purification precipitation in		Precipitation in	
		solution	residue	solution	residue	solution	residue	solution	residue	solution	residue
1	Li	48	52	82	18	93	7	85	15	43	57
	Co	0	100	84	16	93	7	83	17	0	100
	Mn	0	100	80	20	91	9	84	16	0	100
	Ni	0	100	56	44	88	8	84	16	0	100
	Al	15	85	87	13	93	7	12	88	0	100
	Cu	0	100	91	9	88	12	63	37	0	100
	Fe	0	100	84	16	–	–	24	76	2	98
	P	2	98	84	16	92	8	0	100	0	100
2.1	Li	76	24	86	14	92	8	80	20	19	81
	Co	0	100	88	12	92	8	86	14	1	99
	Mn	0	100	88	12	91	9	89	11	5	95
	Ni	0	100	81	19	92	8	81	19	0	100
	Al	10	90	77	23	92	8	26	74	0	100
	Cu	0	100	100*	0	0	100	–	–	–	–
	Fe	0	100	46	54	–	–	9	91	0	100
	P	14.5	85.5	93	7	86	14	9	91	0	100
2.2	Li	33	67	76	24	90	10	65	35	59	41
	Co	0	100	64	36	91	9	33	67	0	100
	Mn	0	100	55	45	91	9	63	37	0	100
	Ni	0	100	52	48	90	10	63	37	0	100
	Al	15	85	100*	0	91	9	9	91	0	100
	Cu	0	100	88	12	87	13	41	59	0	100
	Fe	0	100	82	18	–	–	15	85	0	100
	P	2	98	81	19	91	9	0	100	–	–
3.1	Li	7	93	83	17	89	11	59	41	69	31
	Co	0	100	64	36	84	16	55	45	0	100
	Mn	0	100	77	23	94	6	55	45	0	100
	Ni	0	100	31	69	93	7	54	46	0	100
	Al	23	77	100*	0	88	12	10	90	0	100
	Cu	0	100	85	15	88	12	29	71	0	100
	Fe	0	100	84	16	–	–	9	91	0	100
	P	0	100	15	85	100*	0	0	100	–	–
3.2	Li	67	33	72	28	88	12	96	4	60	40
	Co	0	100	65	35	89	11	90	10	0	100
	Mn	0	100	98	2	89	11	94	6	0	100
	Ni	0	100	54	46	88	12	90	10	0	100
	Al	3	97	60	40	83	17	37	63	0	100
	Cu	0	100	85	15	5	95	41	59	0	100
	Fe	0	100	52	48	–	–	0	100	–	–
	P	3	97	48	52	71	29	0	100	–	–

*) Analytical results were adjusted to maximal value possible due to analytical deviations.

Appendix B. . Material prices and parameters

.

Table 7
Impurity levels in battery-grade materials (own table).

Elemente	Li_2CO_3 *1	LiOH *2	$NiSO_4 \cdot 6H_2O$ *3	$CoSO_4 \cdot 7H_2O$ *3	$MnSO_4 \cdot xH_2O$ *3
	ppm	ppm	pmm	pmm	ppm
Ni	< 30	< 5	–	< 300	< 30
Co	–	–	< 10	–	< 500
Mg	< 100	< 5	< 10	< 1500	< 100
Na	< 250	< 20	< 50	< 10	< 200
Ca	< 50	< 20	< 5	< 2000	< 100
Fe	< 20	< 5	< 10	< 25	< 50
Cu	< 10	< 5	< 5	< 100	< 100
Zn	< 10	–	< 5	< 5	< 20
Mn	< 10	< 5	< 10	< 300	–
Cd	–	–	< 5	< 10	< 5
Pb	< 10	–	< 10	< 10	–
Cr	–	< 5	< 10	< 5	–
K	< 10	< 10	–	–	–
S	< 800	< 20	–	–	–
Cl	–	< 15	–	–	–

*1) Huarui Metal; *2) Halmek Lithium; *3) Targray.
https://halmeklithium.com/en/our_production/lithium-hydroxide/lithium-hydroxide-high-purity-grade/ Aufgerufen: 11.08.2025.
https://www.hruimetal.com/high-purity-999-battery-grade-li2co3-powder-lithium-carbonate-powder-product/ Aufgerufen: 11.08.2025.
https://www.targray.com/li-ion-battery/cathode-materials/nickel-sulphate Aufgerufen: 11.08.2025.
https://www.targray.com/li-ion-battery/cathode-materials/cobalt-sulphate Aufgerufen: 11.08.2025.
https://www.targray.com/li-ion-battery/cathode-materials/manganese-sulphate Aufgerufen: 11.08.2025.

Table 8
Material prices and parameters of the price development scenarios (own table).

Material j	Price p_j		Price growth rate g_j		
	Initial value		Lower scenario	Base scenario	Upper scenario
Steel scrap	359.10	€/t	0.02330	0.03965	0.05141
Cu scrap	7,253.20	€/t	0.03125	0.04760	0.05936
Al scrap	1,745.34	€/t	0.01182	0.02817	0.03993
Li_2CO_3	17,235.81	€/t	0.07189	0.08824	0.10000
C (graphite)	1,225.99	€/t	0.05082	0.06717	0.07893
$Co(OH)_2$	17,823.68	€/t	0.00000	0.00883	0.02059
$Mn(OH)_2$	5,572.10	€/t	0.01830	0.03465	0.04641
$Ni(OH)_2$	18,905.27	€/t	0.01546	0.03181	0.04357
N_2	0.17	€/m^3	0.03501	0.05136	0.06312
Water	1.58	€/t	0.00000	0.01635	0.02811
NaOH	946.05	€/t	0.05384	0.07019	0.08195
H_2O_2	619.57	€/t	0.00000	0.01563	0.02739
H_2SO_4	104.95	€/t	0.04769	0.06404	0.07580
Fe powder	2,279.68	€/t	0.03239	0.04874	0.06050
Waste (solid) disposal	96.48	€/t	0.00000	0.01505	0.02681
Electrolyte disposal*	340.00	€/t	0.00000	0.01635	0.02811
Al/Fe hydroxide disposal*	50.00	€/t	0.00000	0.01635	0.02811
Wastewater treatment*	50,000.00	€/a	0.00000	0.01635	0.02811
Electricity (2–20 GWh)	248.20	€/MWh	0.03795	0.05430	0.06606

*) Based on own experience.

Appendix C. . Details of process steps from the TCO model

.

Table 9
Main components of technical equipment (own table).

Process step	Technical equipment (main components)
Presorting	X-ray transmission sorting line including conveyor belts; air pressure system
Mechanical treatment	Machines for size reduction and screening; auxiliary equipment for processing
Thermal treatment	Rotary kiln (heating system, infrastructure for gases/electricity)
Hydrometallurgy	Reactors (agitator, heating system, pumping system); filter press

Table 10
Allocation of the initial investment to the process steps including presorting (own table).

Process step	Buildings	Technical equipment	Sum
Presorting	0.61 %	1.47 %	2.08 %
Mechanical treatment	4.69 %	2.10 %	6.79 %
Thermal treatment	4.67 %	7.90 %	12.57 %
Hydrometallurgy	36.75 %	41.81 %	78.56 %
Sum	46.72 %	53.28 %	100.00 %

Table 11
Labor costs by process step (own table).

Process step	Number of employees	Annual labor costs
Presorting	2	343,330.23 €
Mechanical treatment	4	686,660.45 €
Thermal treatment	3	514,995.34 €
Hydrometallurgy	5	858,325.56 €
General tasks	6	1,029,990.68 €
Sum	20	3,433,302.25 €

Table 12
Overview of relevant variable costs and revenues per process step (own table).

Process step	Variable cost types	Revenue types
Presorting	Energy	None
Mechanical treatment	Material (water), energy, disposal	Marketable outputs (scrap: steel, copper, aluminum)
Thermal treatment	Material (water, N_2, NaOH), energy, disposal	None
Hydrometallurgy	Material (water, NaOH, H_2O_2, H_2SO_4, Fe powder), energy, disposal	Marketable outputs (Li_2CO_3, graphite, Ni/Mn/Co hydroxide)

Table 13
Shares of cost categories and process steps in total costs across price development scenarios (own table).

Cost category	LIBZ1	LIBZ2	LIBZ3
Capex	11.94 % – 17.99 %	11.75 % – 17.68 %	11.66 % – 17.58 %
Material	24.43 % – 31.35 %	24.73 % – 32.01 %	25.15 % – 32.55 %
Energy	32.54 % – 39.77 %	31.52 % – 38.60 %	31.35 % – 38.30 %
Disposal	1.50 % – 1.85 %	1.45 % – 1.80 %	1.43 % – 1.77 %
Maintenance	2.83 % – 4.26 %	2.79 % – 4.19 %	2.77 % – 4.17 %
Insurance	1.23 % – 1.86 %	1.21 % – 1.82 %	1.20 % – 1.81 %
Labor	11.32 % – 17.07 %	12.13 % – 18.25 %	12.03 % – 18.15 %
Process step	LIBZ1	LIBZ2	LIBZ3
Sorting	0.00 %	1.82 % – 2.55 %	1.80 % – 2.54 %
Mechanical pretreatment	5.29 % – 7.27 %	5.10 % – 6.99 %	5.06 % – 6.96 %
Thermal pretreatment	5.05 % – 6.82 %	4.86 % – 6.56 %	4.83 % – 6.52 %
Hydrometallurgy	80.22 % – 85.88 %	78.43 % – 84.58 %	78.54 % – 84.70 %
General	3.77 % – 5.69 %	3.64 % – 5.47 %	3.61 % – 5.45 %

.

Appendix D. . Detailed sensitivity analysis charts

The abbreviations used in the figures indicate the presorting scenario and the price development scenario (FP: fixed, LP: lower, BP: base, UP: upper).

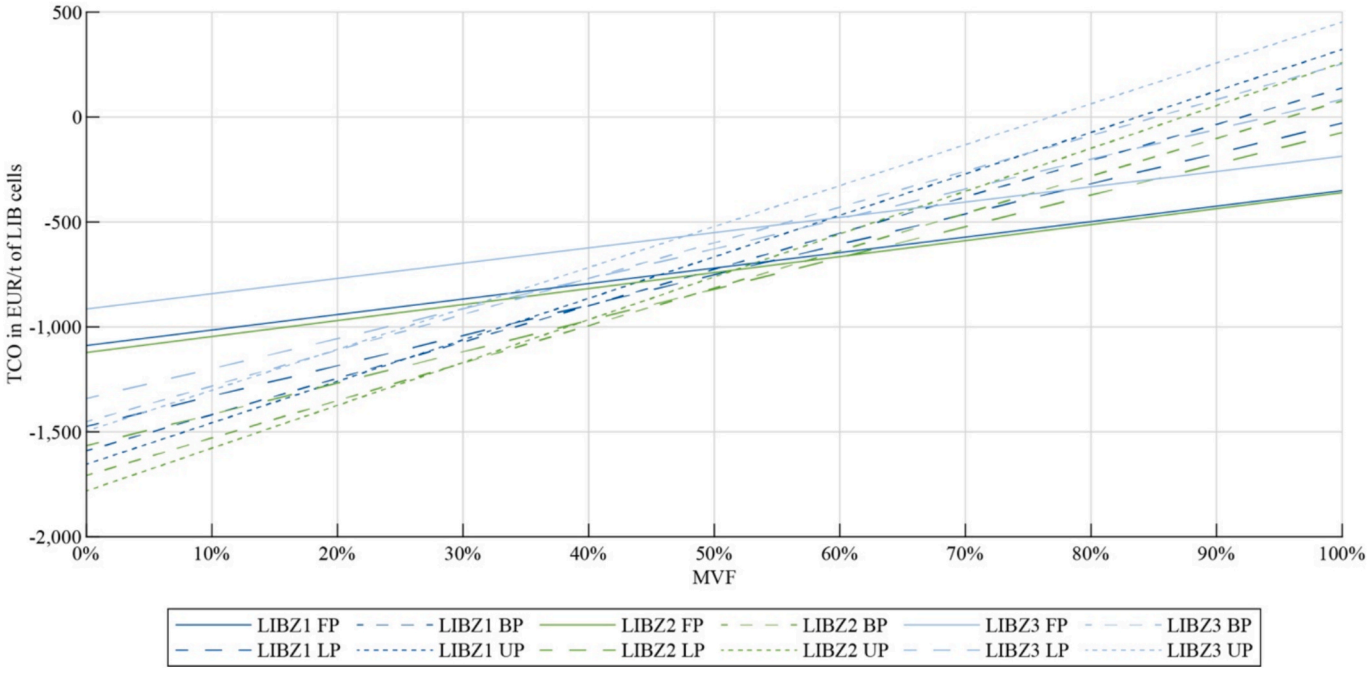

Fig. 5. Impact of the MVF on the TCO per t of LIB cells processed for Li_2CO_3 for all scenarios (own figure).

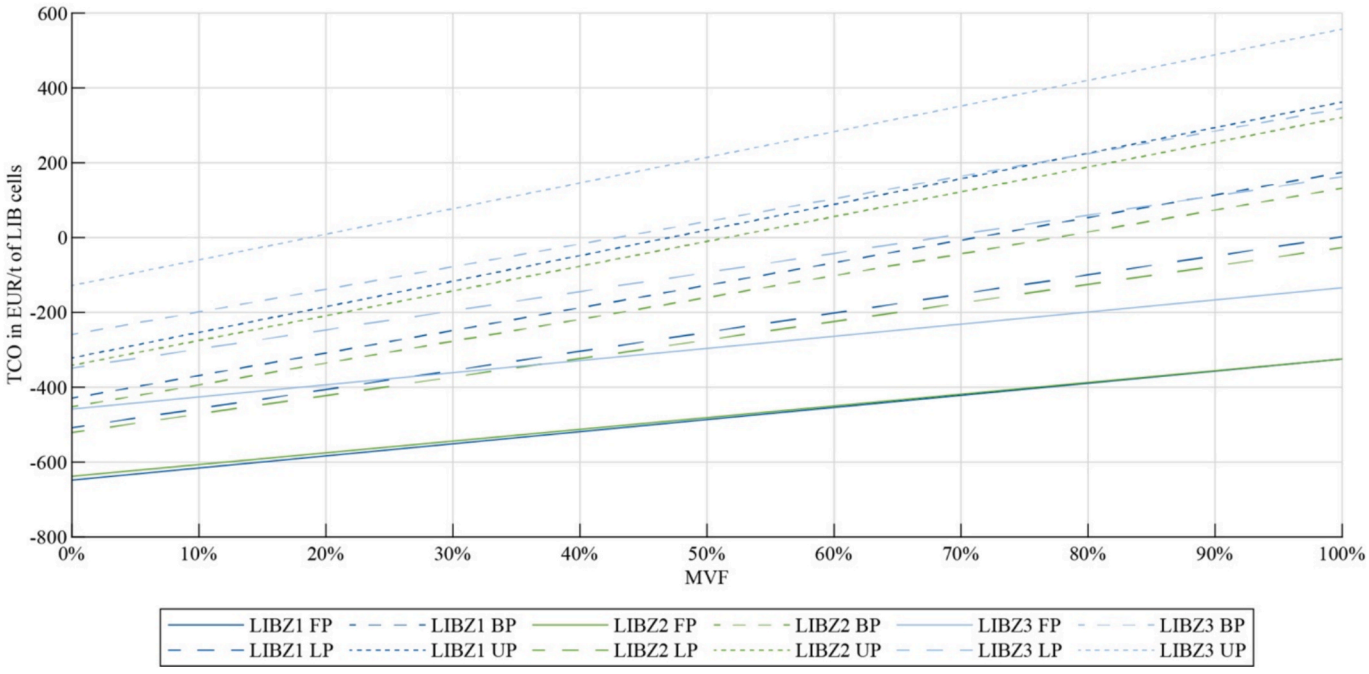

Fig. 6. Impact of the MVF on the TCO per t of LIB cells processed for graphite for all scenarios (own figure).

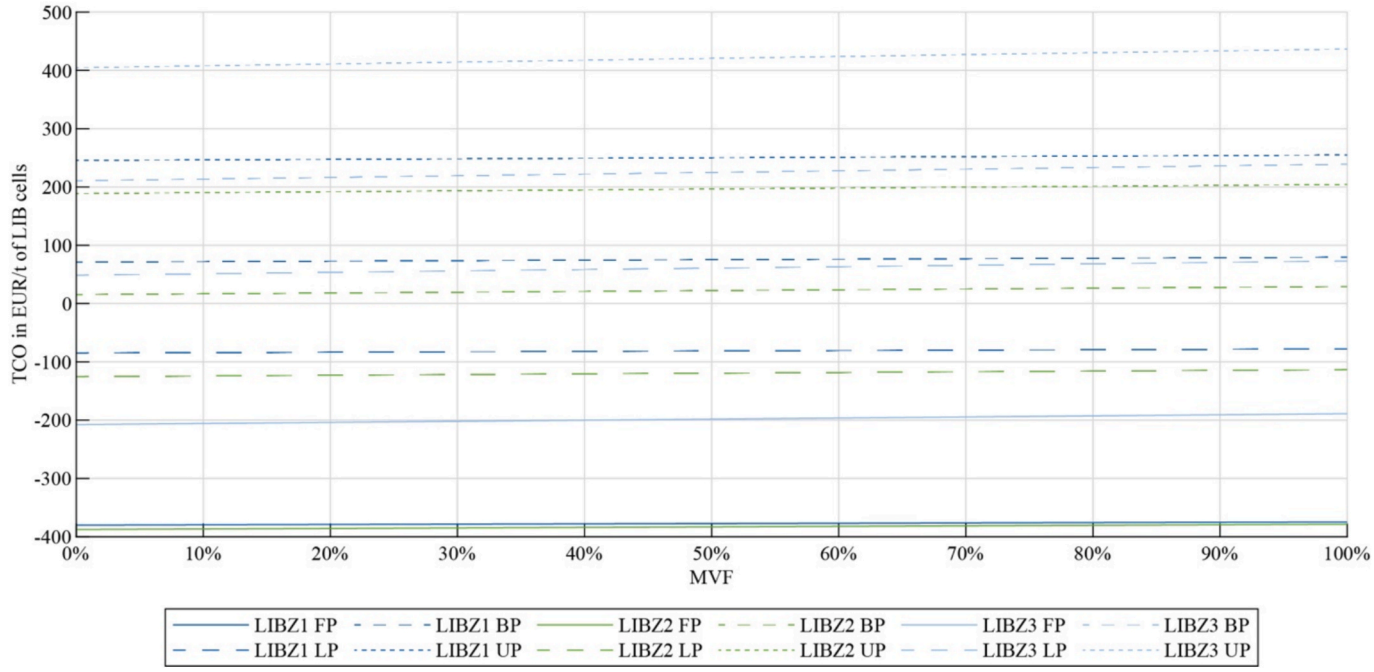

Fig. 7. Impact of the MVF on the TCO per t of LIB cells processed for cement Cu for all scenarios (own figure).

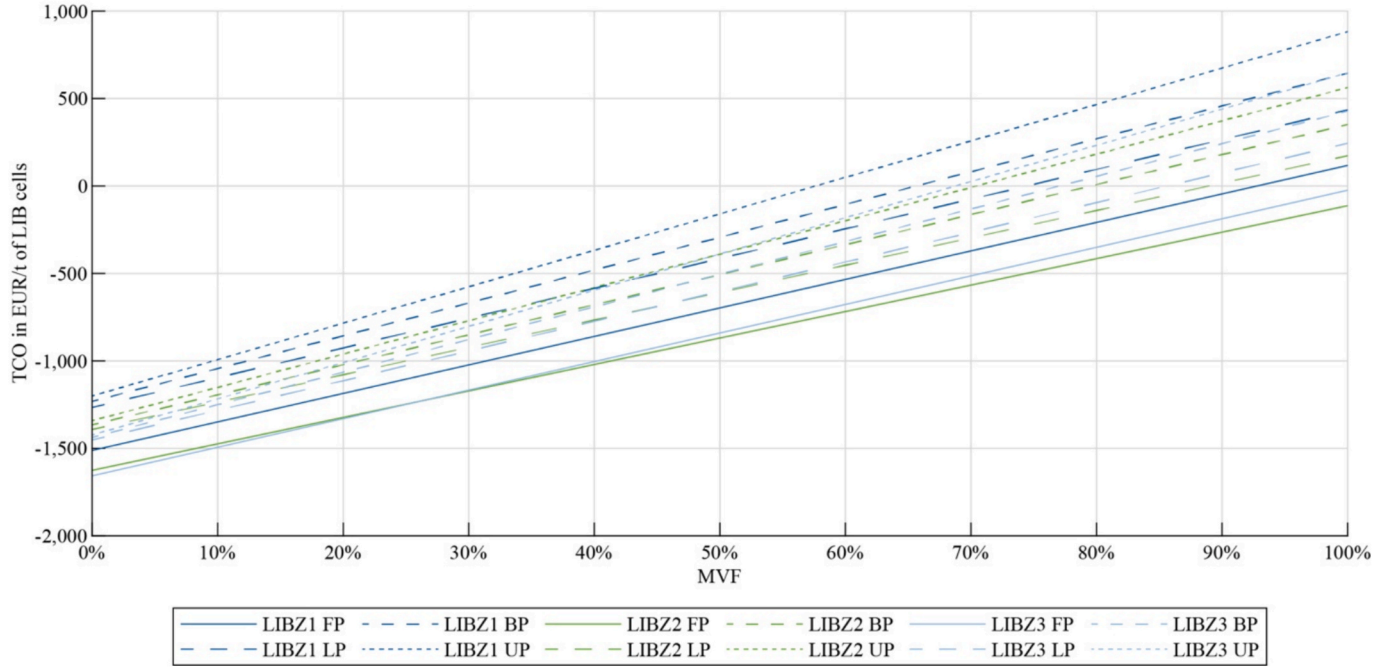

Fig. 8. Impact of the MVF on the TCO per t of LIB cells processed for Ni/Co/Mn hydroxide for all scenarios (own figure).

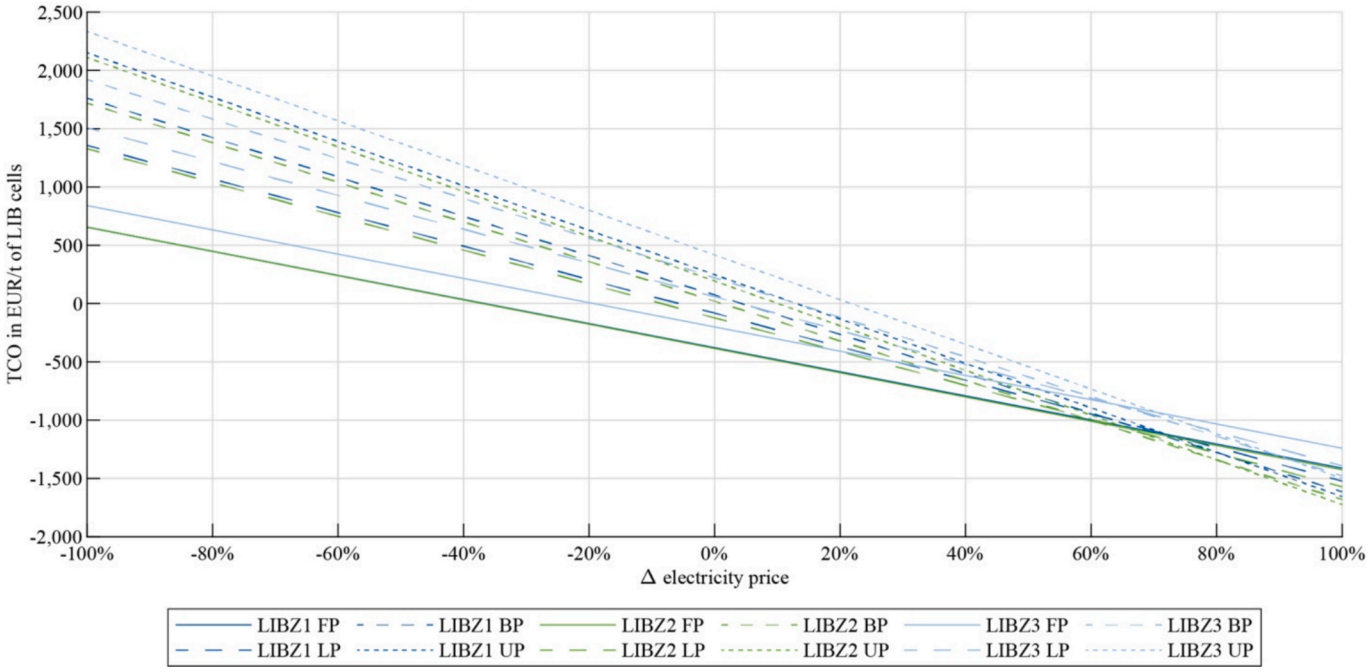

Fig. 9. Impact of changes in the electricity price on the TCO per t of LIB cells processed for all scenarios (own figure).

.

Data availability

Data will be made available on request.

References

Arnberger, A.; Coskun, E.; Rutrecht, B. (2018): Recycling von Lithium-Ionen-Batterien. In Stephanie Thiel, Elisabeth Thomé-Kozmiensky, Daniel Goldmann (Eds.): Recycling und Rohstoffe, vol. 11. Nietwerder: TKh2018 (Recycling und Rohstoffe, 11), pp. 583–599.

Babanejad, S., Ahmed, H., Andersson, C., Samuelsson, C., Lennartsson, A., Hall, B., Arnerlöf, L., 2022. High-temperature behavior of spent Li-ion battery black mass in inert atmosphere. In J. Sustain. Metall. 8 (1), 566–581. https://doi.org/10.1007/s40831-022-00514-y.

Bärwaldt, G., Kwade, A., 2012. LithoRec Recycling von Lithium-Ionen-Batterien. Abschlussbericht zum Verbundvorhaben im Rahmen des FuE-Programms „Förderung von Forschung und Entwicklung im Bereich der Elektromobilität". Cuvillier Verlag, Göttingen.

Bettersize Instruments Ltd. (Ed.) (2021): Improving Lithium-Ion Batteries through Measuring Tapped Density. Available online at https://www.azom.com/article.aspx?ArticleID=21056, updated on 12/8/2021, checked on 4/16/2025.

Bhutta, K.S., Huq, F., 2002. Supplier selection problem: a comparison of the total cost of ownership and analytic hierarchy process approaches. In Supply Chain Manag. 7 (3), 126–135. https://doi.org/10.1108/13598540210436586.

BKI - Baukosteninformationszentrum Deutscher Architektenkammern (2024): Baukosten Gebäude Neubau 2024. Statistische Kostenkennwerte Teil 1. Stuttgart: BKI.

BMG - Bundesministerium für Gesundheit (2024): Bekanntmachung des durchschnittlichen Zusatzbeitragssatzes nach § 242a Absatz 2 des Fünften Buches Sozialgesetzbuch für das Jahr 2022, revised 11/6/2024. Source: BAnz AT 07.11.2024 B4. Available online at https://www.bundesanzeiger.de/pub/publication/lErtX3qtBqz33CLzogK/content/lErtX3qtBqz33CLzogK/BAnz AT 07.11.2024 B4.pdf, checked on 2/18/2025.

Bobba, S., Carrara, S., Huisman, J., Mathieux, F., Pavel, C., 2020. Critical raw materials for strategic technologies and sectors in the EU. A foresight study. Luxembourg: Publ. Off. Eur. Union. https://doi.org/10.2873/58081.

Bundesregierung Deutschland (2018): Verordnung zur Bestimmung der Beitragssätze in der gesetzlichen Rentenversicherung für das Jahr 2018 (Beitragssatzverordnung 2018). BSV 2018, revised 12/18/2017. In *Bundesgesetzblatt Teil I* 2017 (79), p. 3976.

Chen, Q., Lai, X., Gu, H., Tang, X., Gao, F., Han, X., Zheng, Y., 2022. Investigating carbon footprint and carbon reduction potential using a cradle-to-cradle LCA approach on lithium-ion batteries for electric vehicles in China. In J. Cleaner Prod. 369, 133342. https://doi.org/10.1016/j.jclepro.2022.133342.

Degraeve, Z., Labro, E., Roodhooft, F., 2000. An evaluation of vendor selection models from a total cost of ownership perspective. In Eur. J. Oper. Res. 125 (1), 34–58. https://doi.org/10.1016/S0377-2217(99)00199-X.

Degraeve, Z., Roodhooft, F., 1999. Effectively selecting suppliers using total cost of ownership. J. Supply Chain Manag. 35 (1), 5–10. https://doi.org/10.1111/j.1745-493X.1999.tb00050.x.

Destatis - Statistisches Bundesamt (2025a): 51000-0014 Aus- und Einfuhr (Außenhandel): Deutschland, Monate, Warenverzeichnis (8-Steller). Available online at https://www-genesis.destatis.de/genesis/online, checked on 2/17/2025.

Destatis - Statistisches Bundesamt (2025b): 61241-0003 Erzeugerpreisindex gewerblicher Produkte: Deutschland, Jahre, Güterverzeichnis (GP2019 2-/3-/4-/5-/6-/9-Steller/ Sonderpositionen). Available online at https://www-genesis.destatis.de/genesis/online, checked on 3/6/2025.

Bundestag, D., 1989. Das Fünfte Buch Sozialgesetzbuch – Gesetzliche Krankenversicherung. SGB 5, revised 10/23/2024. Bundesgesetzblatt Teil I 1988 (62), 2477.

Bundestag, D., 1995. Das Elfte Buch Sozialgesetzbuch – Soziale Pflegeversicherung. SGB 11, revised 5/30/2024. Bundesgesetzblatt Teil I 1994 (30), 1014.

Bundestag, D., 1997. Das Siebte Buch Sozialgesetzbuch – Gesetzliche Unfallversicherung. SGB 7, revised 10/23/2024. In Bundesgesetzblatt Teil I 1996 (43), 1254.

Bundestag, D., 1998. Das Dritte Buch Sozialgesetzbuch – Arbeitsförderung. SGB 3, revised 10/23/2024. Bundesgesetzblatt Teil I 1997 (20), 594.

Diekmann, J., Hanisch, C., Froböse, L., Schälicke, G., Loellhoeffel, T., Fölster, A.-S., Kwade, A., 2017. Ecological recycling of lithium-ion batteries from electric vehicles with focus on mechanical processes. In J. Electrochem. Soc. 164 (1), A6184–A6191. https://doi.org/10.1149/2.0271701jes.

Ellram, L.M., 1994. A taxonomy of total cost of ownership models. In J. Bus. Logist. 15 (1), 171–191.

Ellram, L.M., 1995. Total cost of ownership: an analysis approach for purchasing. Int. J. Phys. Dist. Logist. 25 (8), 4–23. https://doi.org/10.1108/09600039510099928.

Ellram, L.M., Siferd, S.P., 1993. Purchasing: the cornerstone of the total cost of ownership concept. J. Bus. Logist. 14 (1), 163–184.

EU - European Union (2023): Regulation (EU) 2023/1542 of the European Parliament and of the Council of 12 July 2023 concerning batteries and waste batteries, amending Directive 2008/98/EC and Regulation (EU) 2019/1020 and repealing Directive 2006/66/EC. In *OJEU* 66 (L 191), pp. 1–117.

EU - European Union (2024): Regulation (EU) 2024/1252 of the European Parliament and of the Council of 11 April 2024 establishing a framework for ensuring a secure and sustainable supply of critical raw materials and amending Regulations (EU) No 168/2013, (EU) 2018/858, (EU) 2018/1724 and (EU) 2019/1020. In *OJEU* 67 (L 1252), pp. 1–67.

Eurostat (2025): Electricity prices for non-household consumers - bi-annual data (from 2007 onwards). Eurostat. Available online at https://ec.europa.eu/eurostat/databrowser/view/nrg_pc_205_custom_15450409/default/table?lang=en, updated on 3/26/2025, checked on 4/1/2025. DOI: 10.2908/nrg_pc_205.

Evertz, M., Kasnatscheew, J., Winter, M., Nowak, S., 2019. Investigation of various layered lithium-ion battery cathode materials by plasma- and X-ray-based element analytical techniques. Anal. Bioanal. Chem. 411 (1), 277–285. https://doi.org/10.1007/s00216-018-1441-8.

Ferrin, B.G., Plank, R.E., 2002. Total cost of ownership models: an exploratory study. J. Supply Chain Manag. 38 (3), 18–29. https://doi.org/10.1111/j.1745-493X.2002.tb00132.x.

Geissdörfer, K., Gleich, R., Wald, A., 2009. Standardisierungspotentiale lebenszyklusbasierter Modelle des strategischen Kostenmanagements. Z. Betriebswirt. 79 (6), 693–715. https://doi.org/10.1007/s11573-009-0256-7.

Gnutzmann, M.M., Makvandi, A., Ying, B., Buchmann, J., Lüther, M.J., Helm, B., et al., 2024. Direct recycling at the material level: unravelling challenges and opportunities through a case study on spent Ni-rich layered oxide-based cathodes. Adv. Energy Mater. https://doi.org/10.1002/aenm.202400840.

Hoeber, L., Steinlechner, S., 2021. A comprehensive review of processing strategies for iron precipitation residues from zinc hydrometallurgy. Cleaner Eng. Technol. 4. https://doi.org/10.1016/j.clet.2021.100214. S. 100214.

Hubert, P., Noclain, A., Jradi, S., Chagnes, A., 2025. Optimizing recycling processes for mixed LFP/NMC lithium-ion batteries: a comparative study of acid-excess and acid-deficient leaching. In: Metals 15 (1), S. 74. https://doi.org/10.3390/met15010074.

Hughes (1970): The recovery of copper from synthetic leach solutions with iron powder. Thesis. University of British Columbia, Vancouver. Department of Mineral Engineering. Online verfügbar unter https://open.library.ubc.ca/soa/cIRcle/collections/ubctheses/831/items/1.0081087, zuletzt geprüft am 14.08.2025.

IG Metall (2011): Wie viel Urlaub steht mir zu? Urlaubsdauer und Urlaubsgeld. Available online at https://www.igmetall.de/tarif/tariftabellen/wieviel-urlaub-steht-mir-zu, updated on 11/11/2011, checked on 2/18/2025.

IG Metall (2024a): Metall- und Elektroindustrie: ERA-Monatsentgelte. Available online at https://www.igmetall.de/download/20240809_Metall_Elektroindustrie_ERA_Tabellen_d6bef241cbb5abb6e85c8b754105c229691c6237.pdf, updated on 5/1/2024, checked on 2/18/2025.

IG Metall (2024b): Metall- und Elektroindustrie: Zuschläge für Mehr-, Schicht-, Wechselschicht- und Nachtarbeit. Available online at https://www.igmetall.de/download/20240422_Metall-Elektroindustrie_Zuschlaege_b2dff431864e347fedc484f26045b23d2fa67f12.pdf, updated on 5/1/2024, checked on 2/18/2025.

Jung, J.-C.-Y., Sui, P.-C., Zhang, J., 2021. A review of recycling spent lithium-ion battery cathode materials using hydrometallurgical treatments. J. Energy Storage 35, 102217. https://doi.org/10.1016/j.est.2020.102217.

Krüger, S., Hanisch, C., Kwade, A., Winter, M., Nowak, S., 2014. Effect of impurities caused by a recycling process on the electrochemical performance of Li [Ni0.33Co0.33Mn0.33]O2. J. Electroanal. Chem. 726, 91–96. https://doi.org/10.1016/j.jelechem.2014.05.017.

LME - London Metal Exchange (2025a): LME Cobalt. Available online at https://www.lme.com/Metals/EV/LME-Cobalt, checked on 2/25/2025.

LME - London Metal Exchange (2025b): LME Nickel. Available online at https://www.lme.com/Metals/Non-ferrous/LME-Nickel, checked on 2/25/2025.

Melin, H. E. (2018): Lithium-ion Battery End-of-Life Market Baseline Study. World Economic Forum. Switzerland. Available online at https://coilink.org/20.500.12592/kr041t, checked on 4/10/2025.

Müller, Marius; Obuz, Hüseyin Eren; Keber, Sebastian; Tekmanli, Firat; Mettke, Luka Nils; Yagmurlu, Bengi (2024): Concepts for the Sustainable Hydrometallurgical Processing of End-of-Life Lithium Iron Phosphate (LFP) Batteries. Sustainability 16 (24), S. 11267. DOI: 10.3390/su162411267.

Nitta, N., Wu, F., Lee, J.T., Yushin, G., 2015. Li-ion battery materials: present and future. Mater. Today 18 (5), 252–264. https://doi.org/10.1016/j.mattod.2014.10.040.

Pagnanelli, F., Altimari, P., Colasanti, M., Coletta, J., D'Annibale, L., Mancini, A., et al., 2024. Recycling Li-ion batteries via the Re-synthesis route: improving the process sustainability by using lithium iron phosphate (LFP) scraps as reducing agents in the leaching operation. Metals 14 (11). https://doi.org/10.3390/met14111275. S. 1275.

Petzold, M., Flamme, S., 2025. Sensorbasierte Charakterisierung und Sortierung von Gerätealtbatterien. In: Müll Abfall 2, 65–73. https://doi.org/10.37307/j.1863-9763.2025.02.04.

Petzold, Moritz; Hams, Sigrid; Flamme, Sabine; Zenisch, Maximiliano A; Vahnstiege, Marc; Nowak, Sascha (2024): Recycling Strategies for Spent Consumer Lithium-Ion Batteries.

Petzold, M., Flamme, S., 2024. Recycling strategies for spent consumer lithium-ion batteries. In Metals 14 (2), 151. https://doi.org/10.3390/met14020151.

Pinegar, H., Smith, Y.R., 2019. Recycling of end-of-life lithium-ion batteries, Part I: commercial processes. J. Sustain. Metall. 5 (3), 402–416. https://doi.org/10.1007/s40831-019-00235-9.

PwC - PricewaterhouseCoopers GmbH (2025): Materials. WACC over the last 12 months. Available online at https://pwc-tools.de/kapitalkosten/en/materials/, checked on 4/1/2025.

Qiu, H., Goldmann, D., Stallmeister, C., Friedrich, B., Tobaben, M., Kwade, A., et al., 2024. The InnoRec process: a comparative study of three mainstream routes for spent lithium-ion battery recycling based on the same feedstock. In Sustainability 16 (9), 3876. https://doi.org/10.3390/su16093876.

Reinhart, L., Vrucak, D., Woeste, R., Lucas, H., Rombach, E., Friedrich, B., Letmathe, P., 2023. Pyrometallurgical recycling of different lithium-ion battery cell systems: economic and technical analysis. In J. Cleaner Prod. 416, 137834. https://doi.org/10.1016/j.jclepro.2023.137834.

Saleem, U., Joshi, B., Bandyopadhyay, S., 2023. Hydrometallurgical routes to close the loop of electric vehicle (EV) lithium-ion batteries (LIBs) value chain: a review. J. Sustain. Metall. 9 (3), 950–971. https://doi.org/10.1007/s40831-023-00718-w.

Schmaltz, T. (2023): Recycling of lithium-ion batteries will increase strongly in Europe. Quantity scenarios of lithium-ion batteries for recycling and their origin. Available online at https://www.isi.fraunhofer.de/en/blog/themen/batterie-update/recycling-lithium-ionen-batterien-europa-starke-zunahme-2030-2040.html, updated on 1/19/2023, checked on 4/16/2025.

Sletsgaard, J.; Pedersen, N. H. (2014): Øget ressourcegenvinding ved forbedret karakterisering af affaldsbatterier. Miljøteknologisk udviklings- og demonstrationsprogram 2012. Miljøstyrelsen. Copenhagen (Miljøprojekt, 1627). Available online at https://www2.mst.dk/Udgiv/publikationer/2014/12/978-87-93283-39-8.pdf, checked on 4/15/2025.

Stallmeister, C., Friedrich, B., 2023. Holistic investigation of the inert thermal treatment of industrially shredded NMC 622 lithium-ion batteries and its influence on selective lithium recovery by water leaching. Metals 13 (12), 2000. https://doi.org/10.3390/met13122000.

Stawag - Stadtwerke Aachen AG (2025): Wasserlieferungsabkommen. Preisblatt zur Belieferung mit Wasser. Available online at https://www.stawag.de/fileadmin/stawag/content/Dokumente/Preise_Mwst/PB_Wasserlieferungsabkommen.pdf, checked on 4/1/2025.

Sterkens, W., Diaz-Romero, D., Goedemé, T., Dewulf, W., Peeters, J.R., 2021. Detection and recognition of batteries on X-Ray images of waste electrical and electronic equipment using deep learning. Resour. Conserv. Recycl. 168, 105246. https://doi.org/10.1016/j.resconrec.2020.105246.

Sun, L., Qiu, K., 2011. Vacuum pyrolysis and hydrometallurgical process for the recovery of valuable metals from spent lithium-ion batteries. J. Hazard. Mater. 194, 378–384. https://doi.org/10.1016/j.jhazmat.2011.07.114.

Sziegoleit, H. (2013): Sortierung von Gerätebatterien. In Karl J. Thomé-Kozmiensky, Daniel Goldmann (Eds.): Recycling und Rohstoffe, vol. 6. Neuruppin: TK-Verl. (Recycling und Rohstoffe, 6), pp. 495–504.

Tao, R., Xing, P., Li, H., Wu, Y., Li, S., Sun, Z., 2021. Full-component pyrolysis coupled with reduction of cathode material for recovery of spent LiNixCoyMnzO 2 lithium-ion batteries. ACS Sustain. Chem. Eng. 9 (18), 6318–6328. https://doi.org/10.1021/acssuschemeng.1c00210.

TOMRA - TOMRA Recycling (2021): Relux installiert Tomras X-Tract zur erfolgreichen Batteriesortierung. Available online at https://www.tomra.com/de-de/waste-metal-recycling/media-center/customer-stories/relux-rohstoffe, updated on 12/13/2021, checked on 4/10/2025.

Vortmann-Westhoven, B., Winter, M., Nowak, S., 2017. Where is the lithium? Quantitative determination of the lithium distribution in lithium-ion battery cells: Investigations on the influence of the temperature, the C-rate and the cell type. In J. Power Sources 346, 63–70. https://doi.org/10.1016/j.jpowsour.2017.02.028.

Wen, G., Yuan, S., Dong, Z., Ding, H., Gao, P., 2024. Recycling of spent lithium iron phosphate battery cathode materials: a review. J. Clean. Prod. 474. https://doi.org/10.1016/j.jclepro.2024.143625. S. 143625.

Wett, C., Lampe, J., Görick, D., Seeger, T., Turan, B., 2025. Identification of cell chemistries in lithium-ion batteries: improving the assessment for recycling and second life. Energy AI 19, 100468. https://doi.org/10.1016/j.egyai.2024.100468.

Woeste, R., Drude, E.-S., Vrucak, D., Klöckner, K., Rombach, E., Letmathe, P., Friedrich, B., 2024. A techno-economic assessment of two recycling processes for black mass from end-of-life lithium-ion batteries. Appl. Energy 361, 122921. https://doi.org/10.1016/j.apenergy.2024.122921.

Wu, Y., 2002. Modified natural graphite as anode material for lithium-ion batteries. J. Power Sour. 111 (2), 329–334. https://doi.org/10.1016/S0378-7753(02)00349-X.

Wurm, C.; Öttinger, O.; Wittkämper, S.; Zauter, R.; Vuorilehto, K. (2013): Anodenmaterialien für Lithium-Ionen-Batterien. In Reiner Korthauer (Ed.): Handbuch Lithium-Ionen-Batterien. Berlin, Heidelberg: Springer Berlin Heidelberg, pp. 45–60. doi: 10.1007/978-3-642-30653-2_5.

Yang, Y., Huang, G., Xu, S., He, Y., Liu, X., 2016. Thermal treatment process for the recovery of valuable metals from spent lithium-ion batteries. Hydrometallurgy 165, 390–396. https://doi.org/10.1016/j.hydromet.2015.09.025.

Zhang, H., Yang, Y., Ren, D., Wang, L., He, X., 2021. Graphite as anode materials: fundamental mechanism, recent progress and advances. Energy Storage Mater. 36, 147–170. https://doi.org/10.1016/j.ensm.2020.12.027.

Zhao, G., Wang, X., Negnevitsky, M., 2022. Connecting battery technologies for electric vehicles from battery materials to management. iScience 25 (2), 103744. https://doi.org/10.1016/j.isci.2022.103744.

Zheng, R., Wang, W., Dai, Y., Ma, Q., Liu, Y., Mu, D., et al., 2017. A closed-loop process for recycling LiNi x Co y Mn (1−x−y) O 2 from mixed cathode materials of lithium-ion batteries. Green Energy Envorin. 2 (1), 42–50. https://doi.org/10.1016/j.gee.2016.11.010.

Zheng, R., Zhao, L.i., Wang, W., Liu, Y., Ma, Q., Mu, D., et al., 2016. Optimized Li and Fe recovery from spent lithium-ion batteries via a solution-precipitation method. In: RSC Adv. 6 (49), 43613–43625. https://doi.org/10.1039/C6RA05477C.

Zhu, S., He, W., Li, G., Zhou, X., Zhang, X., Huang, J., 2012. Recovery of Co and Li from spent lithium-ion batteries by combination method of acid leaching and chemical precipitation. Trans. Nonferrous Met. Soc. China 22 (9), 2274–2281. https://doi.org/10.1016/S1003-6326(11)61460-X.

Zou, Yuanmin; Chernyaev, Alexander; Ossama, Muhammad; Seisko, Sipi; Lundström, Mari (2024a): Leaching of NMC industrial black mass in the presence of LFP. *Scientific reports* 14 (1), doi: 10.1038/s41598-024-61569-3. S. 10818.

Zou, Y., Chernyaev, A., Seisko, S., Sainio, J., Lundström, M., 2024b. Removal of iron and aluminum from hydrometallurgical NMC-LFP recycling process through precipitation. Minerals Engineering 218. https://doi.org/10.1016/j.mineng.2024.109037. S. 109037.